Iron Chalcogenide Photovoltaic Absorbers

Liping Yu, Stephan Lany, Robert Kykyneshi, Vorranutch Jieratum, Ram Ravichandran, Brian Pelatt, Emmeline Altschul, Heather A. S. Platt, John F. Wager, Douglas A. Keszler, and Alex Zunger*

Realizing new, efficient solar absorbers containing earth-abundant elements represents a critical component for expanding the reach of photovoltaic (PV) technologies, meeting growing energy needs, and ameliorating atmospheric CO_2 concentrations. Among all of the elements, Fe is ranked fourth in terms of abundance in the earth's crust, and it is the least expensive metallic element to extract from Nature. The use of Fe in PV was proposed more than 25 years ago in the form of FeS_2 pyrite. Unfortunately, the material has been plagued by performance problems that to this day are both persistently present and not well understood. Considering the current level of understanding and the recent resurgence of interest in Fe-bearing PV materials,[1,2] we have undertaken a concerted and integrated theoretical and experimental study that provides new insight into the problem of FeS_2. We use this insight to propose and then implement design rules for identifying new Fe-containing materials. These rules have led us to consider the new materials Fe_2SiS_4 and Fe_2GeS_4, which may well circumvent the limitations of pyrite.

The initial promise of Fool's Gold: In addition to its abundance, FeS_2 exhibits a useful band gap (E_g = 0.9 eV)[3] and an absorption coefficient that rises to a remarkable level above 10^5 cm^{-1} at E_g + 0.1 eV. This high absorption coefficient (as strong as that of organic dyes at visible photon energies!) provides a unique opportunity among inorganic materials to incorporate a very thin absorber layer (<0.1 μm) in a solar cell to capture most of the incident solar radiation. This thickness can be compared to 1.5–3 μm for current thin-film technologies and >200 μm for single-crystal Si cells. Such thin layers not only conserve material, but they also provide an avenue to high efficiency through efficient charge separation associated with a high internal electrical field. But, like its common name, fool's gold, FeS_2 as the promised golden solution for PV has not come true. While the material exhibits exceptional optical and electrical properties, a photo response representative of the intrinsic band gap has not been observed. Single crystals are commonly observed to be *n*-type. In photoelectrochemical cell measurements, the open-circuit voltage, V_{oc}, is generally measured to be a mere 0.01 V, rising to 0.2 V with surface treatments,[4] i.e., well below the measured optical band gap. In contrast, thin films are commonly *p*-type, and they exhibit no photoelectrochemical response. After nearly a decade of effort,[5] work on FeS_2 largely ceased as the PV community turned its attention to thin-film materials such as $Cu(In,Ga)Se_2$[6] and CdTe,[7] spawning technologies that have now reached commercial module production with efficiencies greater than 10 percent.[8] Yet, the toxicity of Cd and scarcity of In continue to pose a threat to these technologies.

The traditional view: Explanations guide materials science, which guides (or misguides) technology. The small V_{oc} in single crystals has commonly been interpreted to reflect S vacancies, which have been proposed to induce energy levels within the band gap[9] and to pin the Fermi level. This model, however, does not directly address the distinctions between *n*-type single crystals and *p*-type films. Since films are more relevant to photovoltaic devices, we focus our effort here on understanding why the films are *p*-type and why they exhibit no photoresponse.

Facile S-vacancy formation in FeS_2 has commonly been invoked to address the observed properties. Such vacancy formation has been supported by various studies, e.g., X-ray diffraction, indicating S deficiency as high as 7.5% (FeS_{2-x}, x = 0.15), and thermogravimetric data, revealing possible S loss on heating to temperatures as low as 400 °C. Indeed, observed *S deficiency* (relative to the ideal FeS_2 stoichiometry) has almost universally been interpreted to imply microscopic *S vacancies* in otherwise perfect FeS_2. The notion that FeS_2 is prone to high S vacancy concentrations is rooted in much earlier unsuccessful attempts to use it as a semiconductor in electronic devices.[3] This model of bulk S vacancies, however, is not without contradictions. Indeed, on the basis of a very careful analysis of the literature, Ellmer and Hopfner[10] have concluded that FeS_2 is actually a stoichiometric compound. Given these contradictory conclusions, the nature of S deficiencies in FeS_2 remains uncertain.

Do bulk S vacancies abound in FeS_2? To address the likelihood that S vacancies can exist in FeS_2, we have calculated the formation energies of all possible isolated and associated intrinsic defects as a function of the chemical potential (reflecting T and pressure-dependent growth conditions such as Fe-rich/S-poor) (**Figure 1**a) and Fermi Energy (Figure 1b) by using density functional theory (see Computational and Experimental Section for details on theory). The defects include Fe vacancy (V_{Fe}), S

Dr. R. Kykyneshi, V. Jieratum, E. Altschul, H. A. S. Platt, Prof. D. A. Keszler
Department of Chemistry
Oregon State University
153 Gilbert Hall, Corvallis, Oregon 97331-4003, USA
E-mail: douglas.keszler@oregonstate.edu
R. Ravichandran, B. Pelatt, Prof. J. F. Wager
School of Electrical Engineering and Computer Science
Oregon State University
1148 Kelley Engineering Center, Corvallis, Oregon 97331-5501, USA
Dr. L. Yu, Dr. S. Lany, Dr. A. Zunger
National Renewable Energy Laboratory
Golden, Colorado 80401, USA

DOI: 10.1002/aenm.201100351

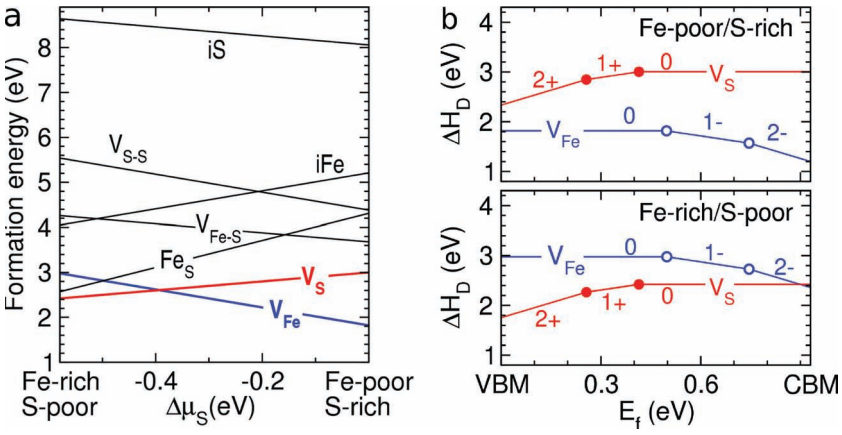

Figure 1. Calculated defect properties of pyrite FeS_2. (a) Formation energies of neutral point defects as a function of the chemical potential. The calculated formation energies of non-bonded Fe-S pair vacancy and non-bonded S-S pair vacancy are higher than their corresponding bonded pair vacancy and are not shown here. (b) Formation energies of charged and neutral defects as a function of E_F for two extreme chemical potential conditions: Upper: Fe poor (S rich) and Lower: extreme Fe rich (S poor) condition. The slope of the line segments (indicated as 0, 1+, 2+, 1– or 2–) represents the defect charge states. The solid dots denote charge transition energies, i.e, values of E_F where transition between charge states occurs. For V_{Fe}, the acceptor (0/1–) and (1–/2–) transition energies are respectively 0.5 eV and 0.75 eV above VBM (E_v). For V_S, the donor transition energies of (2+/1+) and (1+/0) are about E_v+0.26 and E_v+0.41 eV.

vacancy (V_S), bonded as well as nonbonded Fe-S vacancy pair ($V_{Fe\text{-}S}$), bonded as well as nonbonded S-S vacancy pair ($V_{S\text{-}S}$), interstitial Fe (iFe), interstitial S (iS), and Fe-on-S antisite substitution (Fe_S). As shown in Figure 1a, the lowest formation-energy defects are V_{Fe} under S rich/Fe poor conditions with ΔH = 1.82 eV and V_S under S poor (Fe rich) conditions with ΔH = 2.42 eV. One notices immediately that these are rather high formation energies, leading to low equilibrium concentrations of bulk vacancies. Such high vacancy formation energies clearly suggest that FeS_2 is a stoichiometric compound, supporting the most recent stoichiometry measurement.[11]

Do S vacancies pin the Fermi energy? V_S also does not cause E_f pinning in bulk FeS_2. In general, the Fermi level would be pinned around the value at which the charged donors and acceptors have the same formation energies and compensate each other.[12] In this case, attempts to shift E_f to higher (lower) energies in the gap would result in formation of additional acceptors (donors), a process that locks E_f due to negative feedback. In Figure 1b, we see that the formation enthalpy of the positively charged V_S (donor) and the negatively charged V_{Fe} (acceptor) do not intersect in the gap at any of the limiting growth (chemical-potential) conditions, thus V_{Fe} and V_S in bulk do not cause Fermi-level pinning. We conclude that S vacancies are rare in the bulk because of a rather high formation energy. Therefore, these vacancies do not cause Fermi-level pinning, and they are unlikely to be responsible for the small, reported open-circuit voltages.

S deficiency in FeS_2 does not imply S vacancies: Given that FeS_2 does not seem to be prone to bulk point-vacancy formation, we enquire, what is the source of the macroscopic loss of S and its potential effects on PV performance. It turns out that there are a few competing Fe-S crystal structures that are S-deficient, such as troilite FeS and pyrrhotite (FeS_{1+x}, x = 0–1/7).[13] **Figure 2**a shows the calculated Gibbs free energies (ΔG) of pyrite with respect to decomposition to FeS + S (red line) or $Fe_{0.877}S$ +S (blue line), as a function of temperature (T) under a pressure of 1 atm. At T > ~350 K and T > ~ 600 K, pyrite is found to decompose to the S-deficient structures $Fe_{0.877}S$ and FeS, respectively. On the other hand, if pyrite is grown at high T (>600 K), the S-deficient phases can form spontaneously during the annealing process. Figure 2b shows the calculated ground-state formation enthalpies (ΔH) convex hull of such S-deficient bulk phases with respect to the end points FeS (troilite) structure and pyrite FeS_2. We see that all intermediate S-deficient phases, e.g., Fe_9S_{10} and $Fe_{10}S_{11}$, have lower energies than the weighted linear average of the end-points between FeS and FeS_2. Thus, intermediate S-deficient

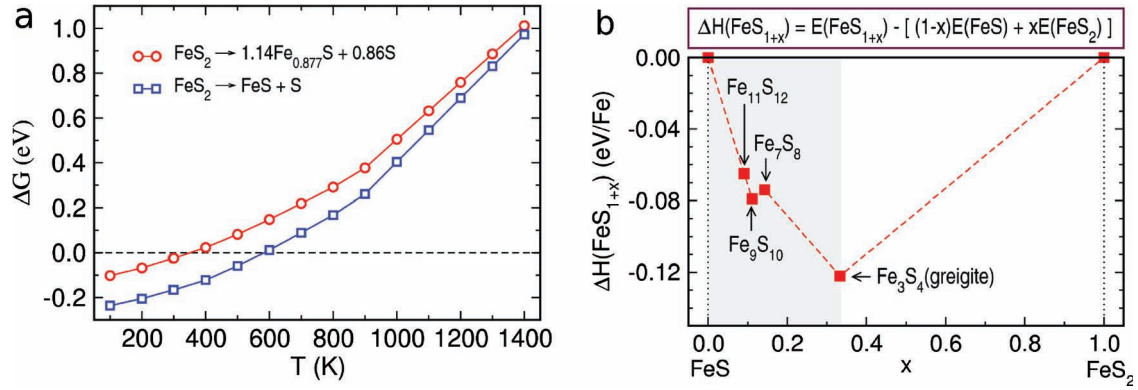

Figure 2. (a) Calculated Gibbs energies of formation of pyrite: $\Delta G = G_{FeS2} - [G_{FeS} + G_S]$ and $\Delta G = G_{FeS2} - [1.14\ G_{Fe0.877S} + 0.86G_S]$ as function of T under the pressure of 1 atm. The free energy G(T) is determined from G(T = 0 K) + [G(T)–G(T = 0 K)], where G(T = 0 K) was calculated from density function theory with U = 1.9 eV and G(T)-G(T = 0 K) is obtained from experimental thermochemical data.[32] The total energy of $Fe_{0.877}S$ was calculated by using Fe_7S_8 structure as an approximation. (b) Calculated formation energy of intermediate S-deficient phases with respect to FeS and FeS_2 at T = 0 K.

phases can form spontaneously if FeS phase is formed during growth, leading to an inhomogeneous microstructure with multiple phases. The coexistence of these S-deficient phases explains the commonly observed S-deficiency,[14,15] consistent with the basic Fe-S phase diagram,[16,17] which shows that these S-deficient phases (mainly FeS and $Fe_{1-x}S$) coexist with pyrite at temperatures from 0 to around 743 °C. Indeed, in both powders and thin films, we commonly observed by X-ray diffraction crystalline, sulfur-deficient secondary phases, e.g., Fe_7S_8 (Figure S2). An overpressure of sulfur vapor is generally required to eliminate evidence of these secondary phases in the X-ray patterns.

Are stable, S-deficient intermediate phases electronically and optically significant? These theoretical findings are further studied by growing thin films via sputtering and solution methods. The films provide an opportunity to test for the existence of S-deficient phases through microstructual analysis as well as electrical and optical measurements. Significantly, both growth methods produce degenerate semiconductors with high carrier concentrations in excess of 10^{19} cm^{-3} (as evidenced by resistivity in the range of 0.1–0.7 Ωcm and Seebeck coefficients near 60 μV/K). Optical transmission for the two types of film are essentially the same ($\alpha = 5 \times 10^5$ cm^{-1} at E_g + 0.3 eV), showing, however, very strong sub-band-gap absorption ($\alpha = 6 \times 10^4$ cm^{-1} at 0.75 eV). High carrier concentrations and high sub-band-gap absorption are common traits of FeS_2 films,[18,19] but their origin has not been directly addressed. To examine the structure of the FeS_2 films in greater detail, we have turned to high-resolution transmission-electron microscopy. As shown in **Figure 3**, crystalline regions of FeS_2 are clearly evident, but they are dispersed through material that is largely amorphous. Chemical analysis via energy dispersive X-ray spectroscopy at random points throughout the film reveals a S-deficient stochiometry with a Fe:S ratio of 1:1.6, despite annealing in a very S-rich environment. The films are thus characterized by crystalline FeS_2 grains (from X-ray diffraction) that are coated by regions of highly sulfur-deficient phases.

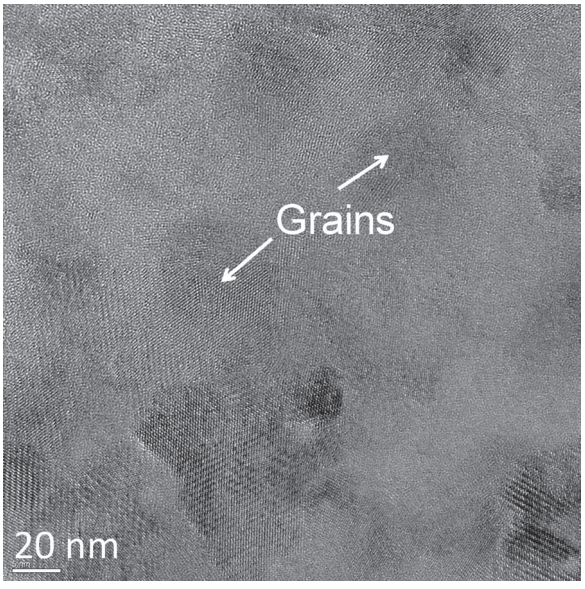

Figure 3. High-resolution transmission electron micrograph of sputtered and annealed FeS_2 thin films.

To further elaborate the nature of the S deficiency and the conductivity of the grain coatings, we have calculated the formation energy for creating a S vacancy in a S-terminated (001) surface. This surface is known to be the most common cleavage plane and predominant growth plane of a natural FeS_2 crystal.[20] The formation enthalpy for a surface V_S is only 0.4 eV, much less than that of a bulk V_S (2.4 eV) under the same S-poor conditions. Hence, V_S can occur much more easily near the surface or grain boundary. In addition, from analysis of the FeS_2-layer projected density of states (Figure S1), we find that the band gap of a defect-free (001) surface is reduced by only 0.3 eV relative to the bulk, wheras a surface layer with V_S becomes metallic, i.e., the band gap is closed (Figure S1). Hence, a low-energy pathway is available for formation of metallic defect-surface coatings and phases, even at modest annealing temperatures, *cf.*, Figure 2.

The picture emerging then is that whereas S vacancies are improbable in the bulk, S deficiencies are readily accommodated through formation of accompanying phases. These phases are known to be metal-like materials.[21] Their presence as largely amorphous forms in the films provides a source of hole carriers. This high carrier concentration in turn leads to free-carrier absorption at energies below the band gap of FeS_2. Despite annealing samples in excess sulfur vapor for an extended period of time at temperatures between 300 and 600 °C, films could not be fully converted to stoichiometric FeS_2. The results are thus consistent with the phase-coexistence results of the calculations, which together with the experiments point to an intrinsic thermal instability of FeS_2 and the considerable challenges that must be surmounted for production of high-quality, single-phase FeS_2 films.

New design principles for Fe–bearing PV absorbers: Our new interpretation forces upon us new "Design Principles". The old design principle of avoiding bulk S vacancies is now replaced by a new insight for identifying Fe sulfides for PV: Select systems that do not spontaneously phase-separate into S deficient conducting materials with small band-gaps. To assure a sufficiently large band gap, the Fe^{2+} ion must be bound by at least six S atoms so as to provide a ligand-field splitting of sufficient magnitude for effective solar absorption. This generally requires Fe^{2+} in an octahedral site. Such a site can be stabilized by adding a third element with an electronegativity that favors strong covalent bonding with sulfur. From these considerations, we have chosen to examine the materials Fe_2MS_4 (M = Si, Ge), noting that Si is second only to Fe in terms of extraction costs from nature.[22]

Properties of Fe_2MS_4 (M = Si, Ge) – no disproportionation into small-gap S deficient structures: These materials have been reported to adopt the olivine structure,[23] which, like pyrite, presents a six-coordinate environment for Fe^{2+}. The disulfide S_2^{2-} unit of FeS_2, however, has been replaced with simple sulfide S^{2-}. We find in our calculations that Fe_2SiS_4 and Fe_2GeS_4 are very stable with respect to decomposition into binaries FeS and SiS_2 (or GeS_2). Our calculated reaction enthalpy, ΔH, for $Fe_2SiS_4 = 2FeS + SiS_2$ and $Fe_2GeS_4 = 2FeS + GeS_2$ are +0.59 eV and +0.64 eV, respectively, meaning the ternaries are more stable than the combination of the corresponding binaries.

From TGA measurements, we find that Fe_2GeS_4 and Fe_2SiS_4 begin to lose mass only above 725 and 1000 °C, respectively. The former mass loss corresponds to the volatilization of GeS_2, while the latter is correlated with the volatilization of SiS_2. The formation of Fe_2GeS_4 thin films by sputtering is confirmed by X-ray diffraction (Figure S3) and electron-probe microanalysis (S/Fe = 1.96, Ge/Fe = 0.51). They exhibit a resistivity of 2.3 kΩ cm and *p*-type majority carriers. This resistivity is similar to that measured on single crystals, *i.e.*, 840 Ω cm, where a carrier concentration of 5×10^{18} cm^{-3} is estimated from the measured Seebeck coefficient of +750 μV/K.[24] Unlike FeS_2, the characteristics of the bulk powders and thin films are equivalent, and they support the calculations with respect to phase stability. The ternary compounds do not readily decompose into *metallic* S-deficient binary phases. This material choice then satisfies the new design principle.

Are the band gap and absorption suitable for PV? The band structure for Fe_2SiS_4 (**Figure 4**a) reveals a valence band dominated by S character and a conduction band dominated by Fe character. The direct gaps calculated for Fe_2SiS_4 and Fe_2GeS_4 are 1.55 and 1.40 eV, respectively. These values compare well to the direct gaps, 1.54 and 1.36 eV (Figure 4b), measured by diffuse reflectance from pressed pellets of Fe_2SiS_4 and Fe_2GeS_4, respectively. An equivalent gap is observed for the Fe_2GeS_4 thin film (Figure S4). All of these band gaps are more than 0.4 eV greater than FeS_2, providing considerable advantages with respect to absorption of the solar spectrum.[25] The optical absorption S 3p → Fe 3d is characterized by a large matrix-transition element, providing the basis for a strong absorption. When coupled with the modest dispersion of the bands and attendant high joint densities of states, absorption coefficients (>10^5 cm^{-1}) approaching that of FeS_2 are predicted (Figure 4c). The Fe_2GeS_4 film also does not exhibit the strong sub band-gap absorption character of FeS_2, again supporting the absence of phase separation and formation of small band-gap binary iron sulfides.

Figure 5 shows the defect formation energies of Fe_2SiS_4 at T ~ 550 K under a pressure of 1 atm. Similar to FeS_2, point vacancy defects have high formation energies. The neutral Fe-on-Si (Fe_{Si}) antisite defect (acceptor), which can be essentially taken as one hole plus $Fe^{3+}{}_{Si}$, has the lowest formation energy, i.e., 0.92 eV. As E_f rises from VBM to CBM, Fe_{Si} and/or V_{Fe} (acceptors) always have lower formation energies than V_S and Si_{Fe} (donors). Hence the carrier concentration of acceptors are always higher than donors, indicating Fe_2SiS_4 is a *p*-type semiconductor, consistent with our experiment. Under equilibrium, Fe_{Si} is incorporated in the 1– charge state, corresponding to a Fe^{3+} oxidation state. The 1– charge is balanced by holes in the valence bands. However, higher in the gap at E_v + 1 eV, Fe_{Si} has a 1–/2– transition where it changes to Fe^{2+}. If Fe_{Si} is abundant, it will trap electrons when the quasi-E_f for electrons comes close to this transition level. Thus, Fe_{Si} could limit V_{oc}, but only around 1 eV above VBM. Realistically, the material is prepared in excess S to force *p*-type behavior, which places the Fermi energy near the VBM, well displaced from an electron concentration favoring the Fe_{Si} defect.

Summary and perspective: The stoichiometry of iron pyrite, FeS_2, has for some time been a controversial topic. Resolving the intrinsic nature of this composition is a key component in understanding the material as a potential photovoltaic absorber. We find from calculations and experimental observations that S deficiencies are a common trait of FeS_2, but they are manifest through coexistence of secondary phases rather than bulk S vacancies in FeS_2. We learn from these findings that deposition of thin films will be a particularly challenging problem. Approaches that rely on high-temperature sintering of high surface -area nanoparticles, for example, are especially problematic.

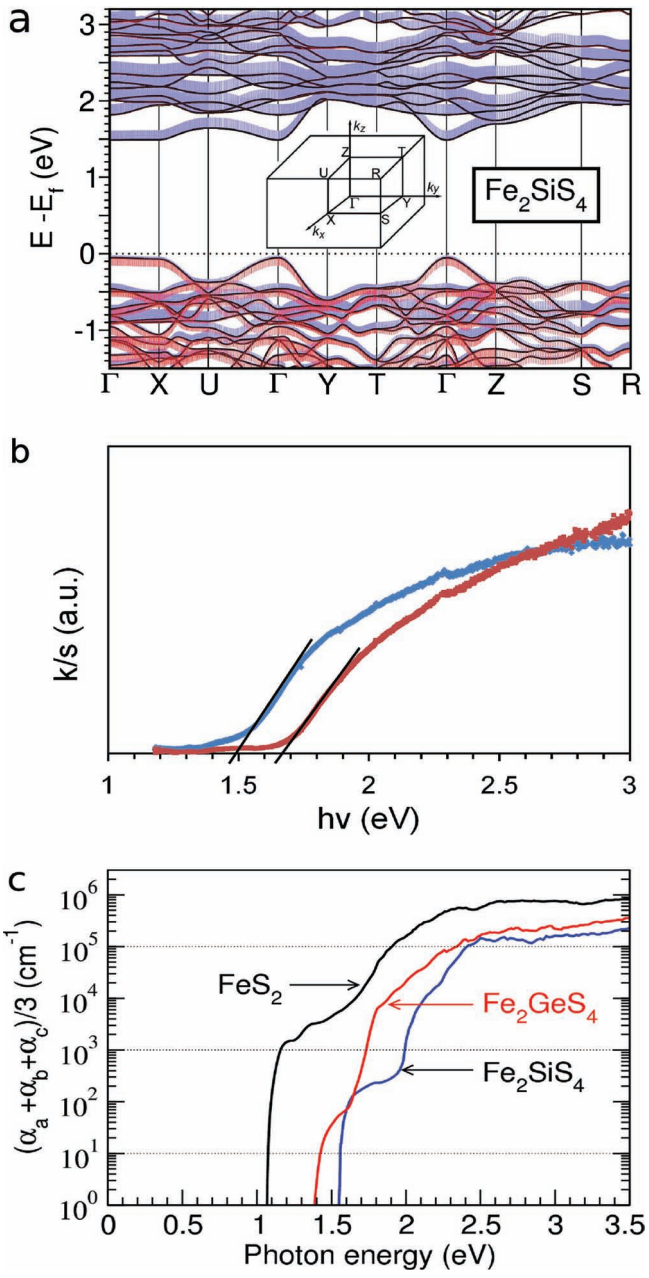

Figure 4. (a) Calculated electronic band structure for Fe_2SiS_4. The widths of the blue and red lines represent the contributions of Fe 3d and S 3p orbitals, respectively, to the bands. (b) Diffuse reflectance data from powders; Fe_2GeS_4–blue line, Fe_2SiS_4–red line. (c) Calculated optical absorption coefficients for FeS_2, Fe_2SiS_4 and Fe_2GeS_4, averaged over three lattice directions up to 3.5 eV.

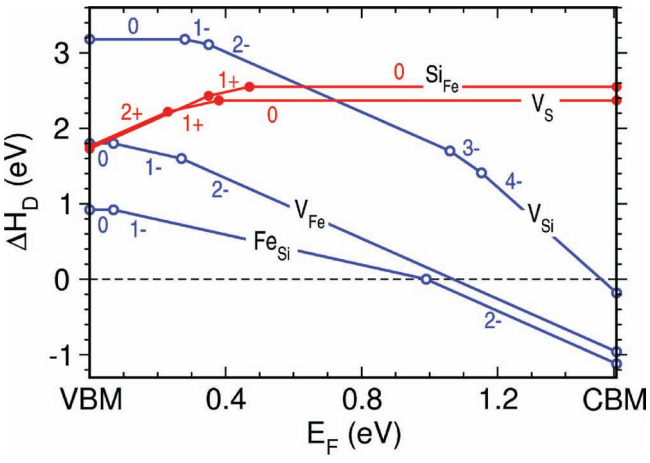

Figure 5. The formation energies of point defects in Fe_2SiS_4 as a function of EF at T ~550K under 1 atm (see Supporting Information for details). The defects Si_{Fe} and V_S, shown by red lines are donors. The blue lines are for acceptors, i.e., V_{Fe}, V_{Si}, and Fe_{Si}.

They will promote phase coexistence, making films unsuitable for realizing the intrinsic properties of FeS_2.

We have been stimulated by the effort on pyrite to formulate design rules for identification of new Fe sulfides that will allow us to avoid the problems of phase coexistence, while retaining attractive optical properties. These rules led us to consider the sulfides Fe_2SiS_4 and Fe_2GeS_4. In comparison to FeS_2, both calculations and experiments indicate that phase coexistence of small band-gap binary iron sulfides is not an issue with these materials. The higher band gaps (1.4–1.5 eV) of the ternaries relative to pyrite (0.9 eV) also provide important advantages with respect to the efficient absorption of the solar spectrum. At the same time, a high absorption coefficient (10^5 cm^{-1}) is retained at E_g + 0.5 eV. In general, defect formation energies are quite high in the materials; their formation should be restricted by using preparative conditions that favor placement of the Fermi energy near the VBM. Hence, considering the current set of calculations and observations, these ternary earth-abundant sulfides represent promising systems for continued development of high-efficiency thin-film solar cells.

Computational and Experimental Section

The calculations are based on density functional theory and plane-wave projector augmented-wave (PAW) method as implemented in the VASP code[26] within the generalized gradient approximation of Perdew, Burke and Ernzerhof (PBE).[27] An energy cutoff of 300 eV was employed. The Hubbard "+U" correction was applied to Fe 3d states (GGA+U), following the simplified rotationally invariant "U" scheme proposed by Dudarev and co-workers.[28] For FeS_2, U = 1.9 eV was chosen, unless specified. At this "U", the lattice parameters, S-S bond length, relative position of d orbitals, and band gap are in good agreement with experimental data. For Fe_2SiS_4 and Fe_2GeS_4, U = 3.9 eV was calculated from linear response theory.[29]

The formation energy of a defect (D) calculated from the formula[10]

$$\Delta H_D^q(E_{F,\mu}) = E_D^q - E_H + \sum \eta_\alpha(\mu_\alpha^0 + \Delta\mu_\alpha) + q(E_\upsilon + E_F),$$

where $E^q{}_D$ and E_H are the total energies of a supercell with and without defect, respectively, and D being in charge state q. n_α is the number of atoms of specie α needed to create a defect. E_F is the Fermi energy relative to VBM (E_v). $\Delta\mu_\alpha$ is the relative chemical potential of specie α with respect to its elemental solid (gas) (μ^0). The relative chemical potentials are taken as variables and are bounded by the values that maintain a stable host compound and avoid formation of all other competing phases (including their elemental solids). In the calculation, supersize effects (image charge interaction, band-filling) and potential alignment have been treated as described elsewhere.[30]

The optical properties are calculated from the complex frequency-dependent dielectric function, which is based on the independent-particle approximation. Quasiparticle self-energy corrections, local-field effects, and excitonic contributions are neglected.[31]

For synthesis of FeS_2, Fe_2GeS_4, and Fe_2SiS_4 samples, mixtures of elemental powders Fe (Cerac, 99.9%), Ge (Alpha Aesar, 99.999%), Si (Alpha Aesar, 99.9985%), and S (Cerac, 99.999%) were mixed and heated in evacuated sealed tubes between 400 and 1000 °C, typically for 48 h. Thermogravimetric analysis was conducted with a Mettler Toledo TGA850 instrument by heating samples in alumina cups under flowing N_2 (g) at 10 °C/min. Single crystals of Fe_2GeS_4 were grown by chemical vapor transport with I_2 (Alpha Aesar 99.99+%) as the transport agent (5 mg/cm^3). Reagents were sealed in evacuated silica tubes (~23 cm long) and placed for three days in a three-zone furnace with the hot zone set to 980 °C and the cold zone at 900 °C. The furnace was then cooled at 5 °C/h to 500 °C, while maintaining the gradient. The power to the furnace was then turned off. Many black needle-shaped crystals, 1–10 mm in length, were found at the end of the tube set in the cold zone.

FeS_2 and Fe_2GeS_4 thin films are deposited by rf magnetron sputtering at room temperature in 5 mTorr Ar/He process gas at 65-W power. The FeS_2 films were annealed under a S atmosphere in a sealed tube at temperatures between 350 and 600 °C for periods of 1 to 15 h. One film was cooled from 550 °C to room temperature at a rate of 12 °C/h. The Fe_2GeS_4 films were annealed with GeS_2 in a sealed tube at a temperature between 600 and 650 °C for 1 h. A precursor for solution deposition of FeS_2 was synthesized by dissolving iron nitrate and elemental iron in a 20/80 water-methanol solution over the course of two days. The resulting solution contained 0.2 M Fe with a NO_3^-/Fe ratio of 2/1. The solvent was then evaporated under flowing argon to produce an iron nitrate gel that was subsequently dissolved in water and spin coated onto both glass and SiO_2/Si substrates. Sulfurization was performed by flowing CS_2(g) over the films during a rapid ramp to 500 °C followed by a one-hour dwell.

Room temperature, 4-point probe resistivity of the films was measured with a LakeShore Cryotronics Hall Measurement System. Seebeck coefficients were measured on a custom-built system with copper electrodes (the reported coefficients are not corrected for the electrode contribution). Optical transmission and reflection as well as diffuse reflectance spectra were collected in the range 1.2–5 eV by using a custom-built spectrometer equipped with an Ocean Optics HR4000 UV-VIS detector and a balanced deuterium/tungsten halogen source (DH-2000-BAL). For the range 0.5–1.4 eV, an Ocean Optics NIR256 detector and a tungsten halogen lamp (Mikropack HL-2000-FHSA) were used.

TEM images were obtained by using an FEI Titan 80-300 TEM, and EPMA data were collected with a CAMECA SX50 electron microprobe (CAMCOR, University of Oregon). Thin-film and powder X-ray diffraction data were obtained with a Rigaku Ultima-IV diffractometer.

Supporting Information

Supporting Information is available from the Wiley Online Library or from the author.

Acknowledgements

This material is based upon work supported by the U.S. Department of Energy, Office of Science, Office of Basic Energy Sciences under Contract

No. DE-AC36-08GO28308 to NREL. The "Center for Inverse Design" is a DOE Energy Frontier Research Center. The Rigaku diffractometer was acquired with funds from the U.S. National Science Foundation under grant no. CHE-0947094.

Received: June 24, 2011
Published online: August 10, 2011

[1] R. Sun, M. K. Y. Chan, G. Ceder, *Phys. Rev. B* **2011**, *83*, 235311.
[2] J. Puthussery, S. Seefeld, N. Berry, M. Gibbs, M. Law *J. Am. Chem. Soc.* **2011**, *133*, 716–719.
[3] E. D. Palik, *Handbook of Optical Constants of Solids* **3**, p.507 (Academic press, **1998**)
[4] K. Buker, N. Alonso-Vante, H. Tributsch, *J. Appl. Phys.* **1992**, *72*, 5721–5728.
[5] A. Ennaoui, S. Fiechter, Ch. Pettenkofer, N. Alonso-Vante, K. Buker, M. Bronold, Ch. Hopfner, H. Tributsch, *Sol. Energy Mater. Sol. Cells* **1993**, *29*, 289–370.
[6] N. Romeo, N. Canevari, G. Sberveglieri, C. Paorici, L. Zanotti, *Phys. Status Solidi A* **1980**, *60*, K95–K98.
[7] D. A. Cusano, *Solid-State Electron.* **1963**, *6*, 217.
[8] R. Noufi, K. Zweibel, *IEEE 4th World Conference on Photovoltaic Energy Conversion (WCPEC-4)* Waikoloa, Hawaii **2006**.
[9] M. Birkholz, S. Fiechter, A. Hartmann, H. Tributsch, *Phys. Rev. B.* **1991**, *43*, 11926.
[10] K. Ellmer, C. Hopfner, C.*Philos. Mag. A.* **1997**, *75*, 1129–1151.
[11] B. Thomas, T. Cibik, C. Hopfner, K. Diesner, G. Ehlers, S. Fiechter, K. Ellmer, *J. Mater. Sci.: Mater. Electron.* **1998**, *9*, 61–64.
[12] C. Persson, Y.-J. Zhao, S. Lany, A. Zunger, *Phys. Rev. B.* **2005**, *72*, 035211.
[13] F. Li, H. F. Franzen, *J. Solid State Chem.* **1996**, *126*, 108–120.
[14] S. Fiechter, J. Mai, A. Ennaoui, W. Szacki, *J. Cryst. Growth.* **1986**, *78*, 438–444.
[15] G. Smestad, A. Da Silva, H. Tributsch, S. Fiechter, M. Kunst, N. Meziani, M. Birkholz, *Sol. Energy Mater.* **1989**, *18*, 299–313.
[16] S. Kissin, S. D. Scott, *Econ. Geol.* **1982**, *77*, 1739–1754.
[17] E. G. Ehlers, *The Interpretation of Geological Phase Diagrams (+Ephemera)* **1972**.
[18] L. Huang, F. Wang, Z. Luan, L. Meng, *Mater. Lett.* **2010**, *64*, 2612–2675.
[19] D. Lichtenberger, K. Ellmer, R. Schieck, S. Fiechter, *Appl. Surf. Sci.* **1993**, *70/71*, 583–587.
[20] R. Murphy, D. R. Strongin, *Surf. Sci. Rep.* **2009**, *64*, 1–45.
[21] E. Konig, *Landolt-Bornstein, New Series, Group II.* (Ed: K. Hellwege), Springer, Berlin **1966**, p.98.
[22] T. D. Kelly, G. R. Matos, Historical statistics for mineral and material commodities in the United States, U.S. Geological Survey Data Series **2009**, p. 140.
[23] H. Vincent, E. F. Bertaut, W. H. Baur, R. D. Shannon, *Acta Crystallogr., Sect. B: Struct. Crystallogr. Cryst. Chem.* **1976**, *32*, 1749–1755.
[24] H. L. Tuller, A. S. Nowick, *J. Phys. Chem. Sol.* **1977**, *38*, 859–867.
[25] S. M. Sze, K. K. Ng, *Fundamentals of Semiconductor Devices*, 3rd edition, John Wiley and Sons, New Jersey **2007**.
[26] G. Kresse, J. Furthmüller, *Comput. Mater. Sci.* **1996**, *6*, 15–50.
[27] J. Perdew, K. Burke, M. Ernzerhof, *Phys. Rev. Lett.* **1996**, *77*, 3865–3868.
[28] S. L. Dudarev, G. A. Botton, S. Y. Savrasov, C. J. Humphreys, A. P. Sutton, *Phys. Rev. B.* **1998**, *57*, 1505–1509.
[29] M. Cococcioni, S. de Gironcoli, *Phys. Rev. B.* **2005**, *71*, 035105–035120.
[30] S. Lany, A. Zunger, *Phys. Rev. B.* **2008**, *78*, 235104–235128.
[31] B. Adolph, J. Furthmüller, F. Bechstedt, *Phys. Rev. B.* **2001**, *63*, 125108.
[32] M. W. Chase Jr., C. A. Davies, J. R. Downey Jr., D. J. Frurip, R. A. McDonald, A. M. Syverud, A. N. *JANAF Thermochemical Tables, 3rd edition, J. Phys. Chem. Ref. Data* **1985**, 14, suppl. 1.